Experimental test of uncertainty relations for quantum mechanics on a circle

J. Řeháček,[1] Z. Bouchal,[1] R. Čelechovský,[1] Z. Hradil,[1] and L. L. Sánchez-Soto[2]

[1]*Department of Optics, Palacky University, 17 listopadu 50, 772 00 Olomouc, Czech Republic*
[2]*Departamento de Óptica, Facultad de Física, Universidad Complutense, 28040 Madrid, Spain*
(Received 19 December 2007; published 24 March 2008)

We rederive uncertainty relations for the angular position and momentum of a particle on a circle by employing the exponential of the angle instead of the angle itself, which leads to circular variance as a natural measure of resolution. Intelligent states minimizing the uncertainty product under the constraint of a given uncertainty in angle or in angular momentum turn out to be given by Mathieu wave functions. We also discuss a number of physically feasible approximations to these optimal states. The theory is applied to the orbital angular momentum of a beam of photons and verified in an experiment that employs computer-controlled spatial light modulators at both the state preparation and analyzing stages.

I. INTRODUCTION

Despite the central role that angular variables play in classical physics, their proper definition in quantum mechanics is beset by difficulties and requires more care than perhaps might be expected [1–3]. Consider, for instance, the simple example of a particle moving on a circle of unit radius: problems essentially arise from the periodicity, which prevents the existence of a well-behaved angle operator, but not of its complex exponential, which we shall denote by $\hat{E}$.

In quantum optics, this issue is by no means purely academic: it turns out to be crucial for a proper understanding of, e.g., the orbital angular momentum (OAM) of light [4]. Indeed, as put forward by Allen and co-workers [5], the Laguerre-Gauss modes, typical of cylindrical symmetry, carry a well-defined OAM per photon. Since it is surprisingly simple to generate, control, filter, and detect OAM states of light experimentally, researchers have begun to appreciate their practical potential for classical [6–8] and quantum information applications [9–15].

Intimately linked to the issue of a proper angle description is the question of the associated uncertainty relations. Surprisingly enough, some subtle aspects of these relations still remain under discussion. From previous work in this topic [16–25] it seems clear that, if one insists on using an angle operator, special care must be taken when using the standard variance, since this is a nonperiodic measure of spread that makes the angular uncertainty depend on the 2π window chosen. Moreover, the associated commutation relation depends on the value of the angle distribution at a point, which makes handling it somewhat cumbersome.

By precise measurements on a light beam, a detailed test of the uncertainty principle for angle and angular momentum has been recently demonstrated [26,27]. The idea is to pass the beam through an angular aperture and measure the resulting angular-momentum distribution [28]. In the same vein, we have presented experimental results [29] that strengthen the evidence that $\hat{E}$ furnishes a correct description of angular phenomena. When a sensible periodic resolution measure (namely, the circular variance) is employed, the associated intelligent states should minimize two inequalities (one for the cosine and the other for the sine), and both cannot be saturated simultaneously. To bypass this drawback, we have looked at the more physically meaningful notion of constrained intelligent states; that is, states that minimize the uncertainty product for a given spread either in angle or in angular momentum. In fact, these states prove to be Mathieu wave functions, which have been attracting great interest in relation to nondiffracting optical fields [30–32].

In this paper, we go one step further and present an improved experimental setup (that uses computer-controlled spatial light modulators at both the state preparation and analyzing stages) to verify in great detail the properties of these constrained intelligent states. As a by-product, we also show that $\hat{E}$ can be associated with a feasible transformation (a forklike hologram) that shifts the values of the angular momentum. Our formulation paves thus the way for a full quantum processing of vortex beams and provides a bridge between the classical theory of singular optics and the realm of quantum optics.

The plan of this paper is as follows. In Sec. II we provide a comprehensive quantum treatment of angular variables, including a discussion about the associated coherent and intelligent states, as well as various suboptimal states. A feasible optical realization of the system under study is provided in Sec. III, with special emphasis on the detection of the angular-momentum spectrum. In Sec. IV our setup is shown and experimental results are presented and discussed at length. Finally, a summary of our achievements and suggestions for possible future upgrades are given in Sec. V.

II. THEORY

A. Quantum description of rotation angles

We consider rotations by an angle ϕ generated by the angular momentum along the z axis, which for simplicity we shall denote henceforth as L. Classically, a point particle is necessarily located at a single value of the periodic coordinate ϕ, defined within a chosen window, e.g., $[0, 2\pi)$. The corresponding quantum wave function, however, is an object extended around the unit circle $\mathbb{S}_1$ and so can be directly affected by the nontrivial topology.

If we treat ϕ as a continuous variable, the Poisson bracket for the angle and the angular momentum is

$$\{\phi, L\} = 1. \tag{2.1}$$

Direct application of the correspondence between Poisson brackets and commutators suggests the commutation relation (in units $\hbar = 1$)

$$[\hat{\phi}, \hat{L}] = i. \tag{2.2}$$

One is tempted to interpret $\hat{\phi}$ as multiplication by ϕ, and then to represent $\hat{L}$ by the differential operator

$$\hat{L} = -i \frac{d}{d\phi} \tag{2.3}$$

which verifies the fundamental relation (2.2). However, the use of this operator may entail many pitfalls for the unwary: single-valuedness restricts the Hilbert space to the subspace of 2π-periodic functions, which, among other things, rules out the angle coordinate as a *bona fide* observable [33–35]. A possible solution, proposed by Judge and Lewis [36], is to modify the angle operator so that it corresponds to multiplication by ϕ plus a series of step functions that sharply change the angle by 2π at appropriate points, which coincides with the classical Poisson bracket of L and a periodic variable.

Many of these difficulties can be avoided by simply selecting instead angular coordinates that are both periodic and continuous. However, a single such quantity cannot uniquely specify a point on the circle because periodicity implies extrema, which excludes a one-to-one correspondence and hence is incompatible with uniqueness. Perhaps the simplest choice [37,38] is to adopt two angular coordinates, such as, e.g., cosine and sine. In classical mechanics this is indeed a good definition, while in quantum mechanics one would have to show that these variables (which we shall denote by $\hat{C}$ and $\hat{S}$ to make no further assumptions about the angle itself) form a complete set of commuting operators. One can concisely condense all this information using the complex exponential of the angle $\hat{E} = \hat{C} + i\hat{S}$, which satisfies the commutation relation

$$[\hat{E}, \hat{L}] = \hat{E}. \tag{2.4}$$

In mathematical terms, this formally defines the Lie algebra of the two-dimensional Euclidean group E(2), which is precisely the canonical symmetry group for the cylinder $\mathbb{S}_1 \times \mathbb{R}$ (i.e., the classical phase space of the system under study).

The action of $\hat{E}$ on the angular momentum basis is

$$\hat{E}|m\rangle = |m - 1\rangle, \tag{2.5}$$

and, since the integer m runs from $-\infty$ to $+\infty$, $\hat{E}$ is a unitary operator whose normalized eigenvectors are

$$|\phi\rangle = \frac{1}{\sqrt{2\pi}} \sum_{m=-\infty}^{\infty} e^{im\phi}|m\rangle. \tag{2.6}$$

The intuitively expected relationship of a discrete Fourier pair between angle and angular momentum is an immediate

consequence of Eqs. (2.3) and (2.6). Indeed, denoting $\Psi_m = \langle m|\Psi\rangle$ and $\Psi(\phi) = \langle \phi|\Psi\rangle$, it holds that

$$\Psi(\phi) = \frac{1}{\sqrt{2\pi}} \sum_{m=-\infty}^{\infty} e^{-im\phi}\Psi_m,$$

$$\Psi_m = \frac{1}{\sqrt{2\pi}} \int_0^{2\pi} d\phi \ \psi(\phi) e^{im\phi}. \tag{2.7}$$

There is an appealing physical interpretation beyond the definition of $\hat{E}$. Whereas in the case of (2.2) one thinks in terms of complementarity between two measurable quantities, $\hat{E}$ primarily represents a transformation and (2.4) may be interpreted as the complementarity between measurement and transformation. On the other hand, the action of $\hat{E}$ can be cast also in terms of measurement, since any unitary operator may be generated by an appropriate Hermitian generator. There is a twofold goal in the theory of angular momentum and its conjugate variable: to characterize them either as a transformation or as a measurement. Notice that the pioneering work in Refs. [26] and [27] anticipated the former interpretation.

The role of $\hat{E}$ as a transformation is determined by the action on the basis states (2.5). What should be explained is the possible measurement associated with $\hat{E}$. Although the vectors $|\phi\rangle$ provide an adequate description of angle, one must take into account that realistic measurements are always imprecise. In particular, the measurement of the spectrum would require infinite energy. In other words, the mathematical continuum of angles will always be observed with a finite resolution. In consequence, it could be interesting to extend the previous formalism by including fuzzy, unsharp, or noisy generalizations of the ideal description provided by $\hat{E}$. To this end we shall use positive-operator-valued measures (POVMs), which are a set of linear operators $\hat{\Lambda}(\phi)$ furnishing the correct probabilities in any measurement process through the fundamental postulate that [39]

$$p(\phi) = \mathrm{Tr}[\hat{\varrho}\hat{\Lambda}(\phi)] \tag{2.8}$$

for any state described by the density operator $\hat{\varrho}$. Compatibility with the properties of ordinary probability imposes the requirements

$$\hat{\Lambda}(\phi) \geq 0, \quad \hat{\Lambda}(\phi) = \hat{\Lambda}^\dagger(\phi), \quad \int_0^{2\pi} d\phi \hat{\Lambda}(\phi) = \hat{1}. \tag{2.9}$$

In addition to these basic statistical conditions, some other requisites must be imposed to ensure a meaningful description of the angle as a canonically conjugate variable with respect to $\hat{L}$. We adopt the same axiomatic approach developed previously by Leonhardt *et al.* [40] for the optical phase. First, we require the shifting property

$$e^{i\phi'\hat{L}}\hat{\Lambda}(\phi)e^{-i\phi'\hat{L}} = \hat{\Lambda}(\phi + \phi'), \tag{2.10}$$

which reflects nothing but the basic feature that an angle shifter is an angle-distribution shifter and imposes the following form for the POVM [41]:

$$\hat{\Lambda}(\phi) = \frac{1}{2\pi} \sum_{m,m'=-\infty}^{\infty} \lambda_{m,m'} e^{i(m-m')\phi} |m\rangle\langle m'|. \quad (2.11)$$

We must also take into account that a shift in $\hat{L}$ should not change the phase distribution. But a shift in $\hat{L}$ is generated by $\hat{E}$ since, according to (2.5), it shifts the angular momentum distribution by one step. Therefore, we require as well

$$\hat{E}\hat{\Lambda}(\phi)\hat{E}^{\dagger} = \hat{\Lambda}(\phi), \quad (2.12)$$

which, loosely speaking, is the physical translation of the fact that angle is complementary to angular momentum. This imposes the additional constraint $\lambda_{m+1,m'+1} = \lambda_{m,m'}$, and this means that $\lambda_{m,m'} = \lambda_{m-m'}$. In consequence, Eq. (2.11) can be recast as

$$\hat{\Lambda}(\phi) = \frac{1}{2\pi} \sum_{l=-\infty}^{\infty} \lambda_l^* e^{-il\phi} \hat{E}^l, \quad (2.13)$$

and the conditions (2.9) are now

$$|\lambda_l| \le 1, \quad \lambda_l^* = \lambda_{-l}. \quad (2.14)$$

Expressing $\hat{E}$ in terms of its eigenvectors, we finally arrive at the more general form of the POVM describing the angle variable and satisfying the natural requirements (2.10) and (2.12):

$$\hat{\Lambda}(\phi) = \int_0^{2\pi} d\phi' \mathcal{K}(\phi') |\phi+\phi'\rangle\langle\phi+\phi'|, \quad (2.15)$$

where

$$\mathcal{K}(\phi) = \frac{1}{2\pi} \sum_{l=-\infty}^{\infty} \lambda_l e^{il\phi}. \quad (2.16)$$

The convolution (2.15) shows that this POVM effectively represents a noisy version of the usual projection $|\phi\rangle\langle\phi|$, and the kernel $\mathcal{K}(\phi)$ gives the resolution provided by this POVM.

B. Gaussian distributions on a circle

Experience with quantum mechanics of simple systems, such as the free particle and harmonic oscillator, suggests that Gaussian states can be an important tool for a better understanding of the periodic motion on a circle. Given this, it is remarkable that there is no clear concise definition of the Gaussian distribution on a circle and one can find only vague statements scattered through the literature.

We do not want to enter here into a mathematical treatment, but rather to grasp the properties that make the Gaussian distribution on the line play such a key role in physics, and that we are particularly keen on retaining when constructing its circular counterpart. We itemize the most relevant ones in our view.

(1) The sum of many independent random variables tends to be distributed following a Gaussian distribution.

(2) All marginal and conditional densities of a Gaussian are again Gaussians.

(3) The Fourier transform of a Gaussian is also a Gaussian.

(4) The Gaussian distribution maximizes the Shannon entropy for a fixed value of the variance.

The first property (subject to a few general conditions) is the central-limit theorem and explains the ubiquity of Gaussians in physics: the distribution of the phenomenon under study does not have to be Gaussian because its average will be. The second and third are responsible for the properties that one assigns to Gaussian states in quantum optics. Finally, the last condition bears on the information-based approach to quantum theory, but strongly depends on the definition of entropy we adopt.

In statistics there are two distributions that have been suggested to have good properties on a circle, namely.

$$p_\kappa(\phi) = \frac{1}{2\pi I_0(2\kappa)} \exp[2\kappa\cos(\phi-\mu)], \quad (2.17)$$

$$p_\sigma(\phi) = \frac{1}{\sqrt{2\pi}\sigma} \sum_{k=-\infty}^{\infty} \exp\left[-\frac{1}{2}\frac{(\phi-\mu+2\pi k)^2}{\sigma^2}\right], \quad (2.18)$$

where I_n denotes the modified Bessel function of the first kind. The first one is known as the von Mises distribution, while the second is the wrapped Gaussian. By a trivial application of the Poisson summation formula, we can express the latter as

$$p_\sigma(\phi) = \frac{1}{2\pi} \vartheta_3\left(\phi-\mu \left| \frac{1}{e^{2\sigma^2}}\right.\right), \quad (2.19)$$

where

$$\vartheta_3(\zeta|q) = \sum_{k=-\infty}^{\infty} q^{k^2} e^{2ik\zeta} \quad (2.20)$$

is the third Jacobi theta function [42,43]. For both distributions μ represents the mean direction, while σ and κ are parameters related to the concentration [44].

From the previous checklist, the wrapped Gaussian satisfies properties 1–3, while the von Mises satisfies property 4 when the variance is replaced by its circular version (so it represents the minimally prejudiced angle distribution, given the information constraints [45]). Therefore, it is tempting to side with the former. Additionally, the Jacobi ϑ_3 function is the solution of the diffusion equation on a circle with the initial state being a δ function, which is another way of defining a Gaussian wave function [46]. However, note that, if we take such a route, Gaussian wave functions no longer lead to Gaussian probability distributions (because the square of a ϑ_3 function is not a ϑ_3 function), a limitation that does not apply to the von Mises distribution.

To complete our choices, it is convenient to make a small detour into the question of coherent states [47] (recall that for the harmonic oscillator they are precisely Gaussian wave packets). Possible definitions of coherent states for a particle on a circle have been outlined in the literature [48,49], but they are of very mathematical nature. We prefer to adopt the

ideas of Rembieliński and co-workers [50] and construct co-herent states $|w\rangle$ as eigenstates of the operator

$$\hat{W} = e^{i(\hat{\phi}+i\hat{L})} = e^{-\hat{L}+1/2}\hat{E}, \qquad (2.21)$$

so that

$$\hat{W}|w\rangle = w|w\rangle, \qquad (2.22)$$

where the complex number $w = e^{i\theta-\ell}$ parametrizes the unit cylinder. Note that

$$\hat{W}|m\rangle = e^{m-1/2}|m-1\rangle, \quad \hat{W}^\dagger|m\rangle = e^{m+1/2}|m+1\rangle, \qquad (2.23)$$

with $[\hat{W},\hat{W}^\dagger] = \sinh(1)e^{2\hat{L}}$. The projection of the vector $|w\rangle$ onto the basis $|m\rangle$ gives then

$$w_m = \langle m|w\rangle = w^{-m}e^{-m^2/2}, \qquad (2.24)$$

while in the angular basis the corresponding expression is

$$w(\phi) = \frac{1}{\sqrt{2\pi}}\vartheta_3\left(\frac{1}{2}(\phi-\mu)\,\middle|\,\frac{1}{e^2}\right), \qquad (2.25)$$

where $\mu = \theta + i\ell$.

In consequence, we have found three families of states with interesting properties: (i) states with von Mises prob-ability density Eq. (2.17); (ii) states with wrapped Gaussian *probability* distribution Eq. (2.18); and (iii) coherent states with wrapped Gaussian *amplitude* density Eq. (2.25). Never-theless, leaving aside fundamental reasons, for computa-tional purposes these three families have very similar angular shapes and give almost indistinguishable numerical results. Therefore, sometimes we will use von Mises states because of their simplicity and the possibility of obtaining analytical results.

C. Constrained intelligent states

Coherent states for the harmonic oscillator are also minimum-uncertainty wave packets. Given the analogy of $\hat{W}$ in Eq. (2.23) with the standard annihilation operator, one is tempted to introduce quadraturelike combinations

$$\hat{Q} = \frac{1}{\sqrt{2}}(\hat{W}+\hat{W}^\dagger), \quad \hat{P} = \frac{1}{\sqrt{2}i}(\hat{W}-\hat{W}^\dagger), \qquad (2.26)$$

which satisfy the uncertainty principle

$$(\Delta\hat{Q})^2(\Delta\hat{P})^2 \geq \frac{1}{4}|\langle[\hat{Q},\hat{P}]\rangle|^2, \qquad (2.27)$$

where $(\Delta\hat{A})^2 = \langle\hat{A}^2\rangle - \langle\hat{A}\rangle^2$ is the standard variance. A lengthy calculation [3] shows that the coherent states (2.25) obey (2.27) as an equality and so they are indeed minimum pack-ets for the variables (2.26). In fact, they are also minimum for more intricate uncertainties [23]. However, the problem is that, in contradistinction with the harmonic oscillator, we do not have any clear operational prescription of how to measure the quadratures (2.26), so they give no real physical insight into the statistical description of angle.

Let us then turn back to the general commutation relation (2.4). First, we observe that dealing with angular mean and variance in the ordinary way has drawbacks. Consider, for example, a sharp angle distribution localized at the origin and the same one shifted by π. Despite the fact that the physical information they convey is the same, in the latter case the variance is much bigger. Since angle is periodic but variance is not, it has little meaning to consider the angle measurement itself [51].

In circular statistics one usually calculates the moments of the exponential of the angle [52–55], often referred to as circular moments and giving rise, e.g., to a circular variance

$$\sigma_\phi^2 = 1 - |\langle e^{i\phi}\rangle|^2, \qquad (2.28)$$

where

$$\langle e^{i\phi}\rangle = \int_0^{2\pi} d\phi\, p(\phi)e^{i\phi}, \qquad (2.29)$$

and $p(\phi)$ is the probability density. The circular variance possesses all the good properties expected: it is periodic, the shifted distributions $p(\phi+\phi')$ are characterized by the same resolution, and for sharp angle distributions it coincides with the standard variance since $|\langle e^{i\phi}\rangle|^2 \simeq 1-\langle\phi^2\rangle$. Moreover, it exactly agrees with

$$(\Delta\hat{E})^2 = \langle\hat{E}^\dagger\hat{E}\rangle - \langle\hat{E}^\dagger\rangle\langle\hat{E}\rangle, \qquad (2.30)$$

which is the natural extension of variance for unitary opera-tors [35].

If we use (2.30), the uncertainty relation associated with (2.4) reads

$$(\Delta\hat{E})^2(\Delta\hat{L})^2 \geq \frac{1}{4}[1-(\Delta\hat{E})^2]. \qquad (2.31)$$

Sometimes it proves convenient to express this in terms of the corresponding Hermitian components $\hat{C}$ and $\hat{S}$. We have

$$[\hat{C},\hat{L}] = i\hat{S}, \quad [\hat{S},\hat{L}] = -i\hat{C}, \qquad (2.32)$$

while $[\hat{C},\hat{S}] = 0$, so that

$$(\Delta\hat{C})^2(\Delta\hat{L})^2 \geq \frac{1}{4}|\langle\hat{S}\rangle|^2, \quad (\Delta\hat{S})^2(\Delta\hat{L})^2 \geq \frac{1}{4}|\langle\hat{C}\rangle|^2. \qquad (2.33)$$

Both inequalities depend on the choice of state used to evalu-ate $\langle\hat{C}\rangle$ and $\langle\hat{S}\rangle$. So intelligent states need to be distinguished from minimum-uncertainty states: there are intelligent states for which the right-hand side of Eq. (2.33) is not the obvious minimum value of 0. The condition of intelligence for, say, the first of (2.33), reads

$$(\hat{L}+i\kappa\hat{C})|\Psi\rangle = \mu|\Psi\rangle, \qquad (2.34)$$

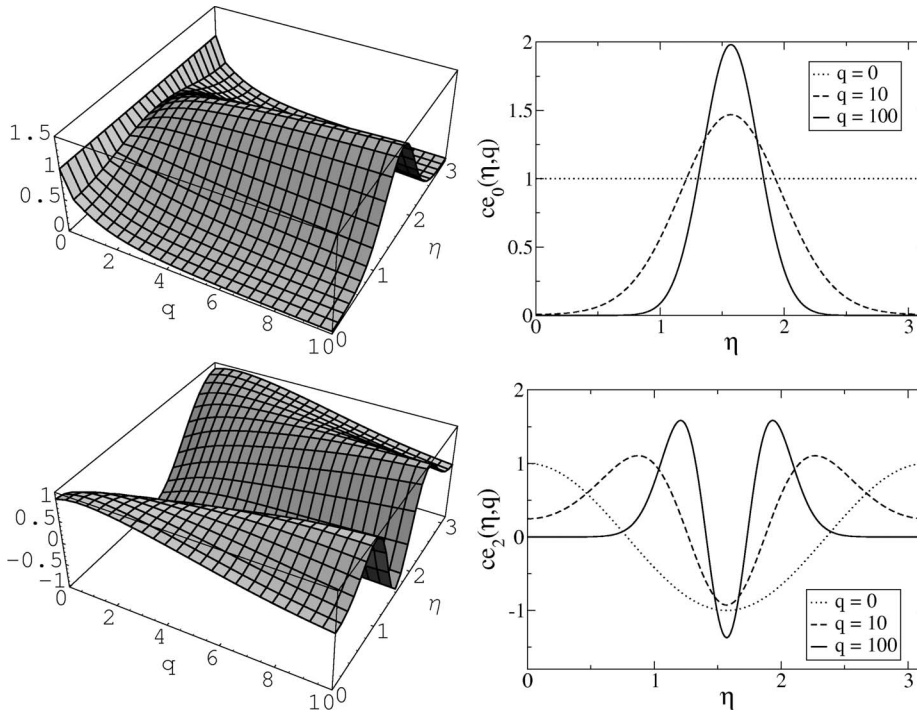which once expressed in the angle representation can be im-mediately solved to give

FIG. 1. Functions $ce_0(\eta,q)$ (top) and $ce_2(\eta,q)$ (bottom). On the right, we show two-dimensional sections of these functions for the values $q=0$, 10, and 100.

$$\Psi(\phi) = \frac{1}{\sqrt{2\pi I_0(2\kappa)}} \exp(i\mu\phi + \kappa \sin\phi), \qquad (2.35)$$

so that the associated probability is the von Mises distribution. The intelligent states for the second equation in (2.33) can be worked out in the same way. However, it is not difficult to prove that both inequalities are saturated simultaneously only for the trivial case of an eigenvector of $\hat{L}$. In other words, the fundamental relation (2.31) is exact, but is too weak.

To get an attainable bound we look instead at normalized states that minimize the uncertainty product $(\Delta\hat{E})^2(\Delta\hat{L})^2$ either for a given $(\Delta\hat{E})^2$ or for a given $(\Delta\hat{L})^2$, which we call constrained intelligent states. We use the method of undetermined multipliers, so the linear combination of variations leads to

$$[\hat{L}^2 + p\hat{L} + (q^*\hat{E} + q\hat{E}^{\dagger})/2]|\Psi\rangle = a|\Psi\rangle, \qquad (2.36)$$

where p, q, and a are Lagrange multipliers. Working in the angle representation, the change of variables $\exp(ip\phi)\Psi(\phi)$ eliminates the linear term from (2.36) (which is equivalent to restricting ourselves to states with zero mean angular momentum). In addition, we can take q to be a real number, since this merely introduces a global phase shift. We finally get

$$\frac{d^2\Psi(\eta)}{d\eta^2} + [a - 2q\cos(2\eta)]\Psi(\eta) = 0, \qquad (2.37)$$

where we have introduced the rescaled variable $\eta=\phi/2$, which has a domain $0 \le \eta < 2\pi$ and plays the role of a polar angle in elliptic coordinates. Equation (2.37) is precisely the standard form of the Mathieu equation, which has many applications not only in optics, but also in other branches of

modern physics [56]. An uncertainty relation of this type has already been investigated by Opatrný [57]. In our case, the only acceptable Mathieu functions are those periodic with period of π or 2π. The values of a in Eq. (2.37) that satisfy this condition are the eigenvalues. We have then two families of independent solutions, namely, the angular Mathieu functions $ce_n(\eta,q)$ and $se_n(\eta,q)$ with $n=0,1,2,\ldots$, which are usually known as the elliptic cosine and sine, respectively. The parity of these functions is exactly the same as their trigonometric counterparts; that is, $ce_n(\eta,q)$ is even and $se_n(\eta,q)$ is odd in η, while they have period π when n is even or period 2π when n is odd. To illustrate these behaviors, in Fig. 1 we have plotted wave functions $ce_n(\eta,q)$ of orders $n=0$ and 2.

Since the 2π periodicity in ϕ requires π periodicity in η, the acceptable solutions for our eigenvalue problem are the independent Mathieu functions $ce_{2n}(\eta,q)$ and $se_{2n}(\eta,q)$, with $n=0,1,\ldots$. In what follows, we consider only even solutions $ce_{2n}(\eta,q)$, although the treatment can obviously be extended to the odd ones with analogous results. We take then

$$\Psi_{2n}(\eta,q) = \sqrt{\frac{2}{\pi}} ce_{2n}(\eta,q), \qquad (2.38)$$

where we have made use of the property

$$\int_0^{2\pi} ce_m(\eta,q)ce_n(\eta,q)d\eta = \pi\delta_{mn} \qquad (2.39)$$
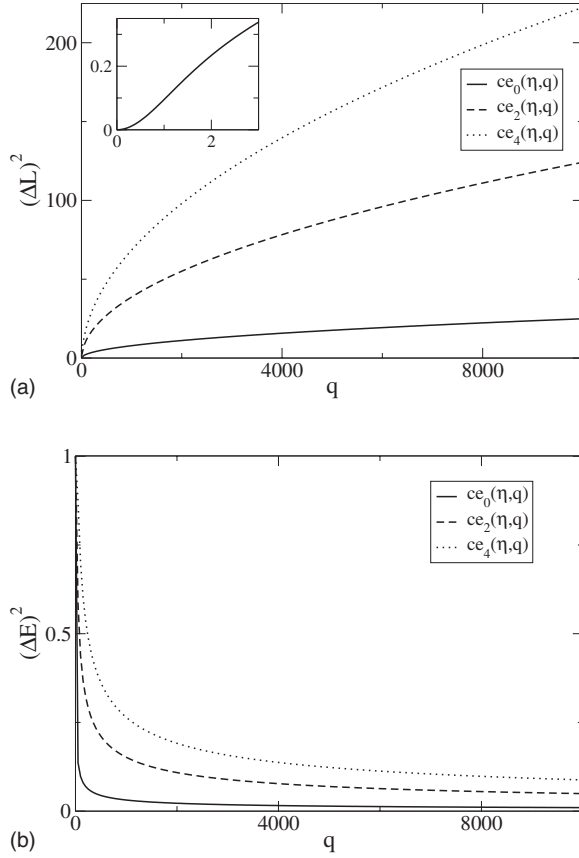
to normalize the wave function. Using (2.38) we have

FIG. 2. $(\Delta\hat{L})^2_{2n}$ and $(\Delta\hat{E})^2_{2n}$ for the three lowest-order wave functions $\Psi_{2n}(\eta,q)$ in terms of the parameter q.

$$(\Delta\hat{L})^2_{2n} = \frac{1}{2\pi}\int_0^\pi d\eta \left(\frac{\partial}{\partial\eta}\mathrm{ce}_{2n}(\eta,q)\right)^2$$

$$= \frac{1}{4}[A^{(2n)}_{2n}(q) - 2q\Theta_{2n}(q)],$$

$$(\Delta\hat{E})^2_{2n} = 1 - \left|\frac{2}{\pi}\int_0^\pi d\eta \ \mathrm{ce}^2_{2n}(\eta,q)\cos(2\eta)\right|^2 = 1 - |\Theta_{2n}(q)|^2.$$
(2.40)

To obtain these analytical expressions we have expanded $\mathrm{ce}_{2n}(\eta,q)$ in Fourier series

$$\mathrm{ce}_{2n}(\eta,q) = \sum_{k=0}^\infty A^{(2n)}_{2k}(q)\cos(2k\eta),$$
(2.41)

and integrated term by term, in such a way that

$$\Theta_{2n}(q) = A^{(2n)}_0(q)A^{(2n)}_2(q) + \sum_{k=0}^\infty A^{(2n)}_{2k}(q)A^{(2n)}_{2k+2}(q).$$
(2.42)

The coefficients $A^{(2n)}_{2k}$ determine the Fourier spectrum and satisfy recurrence relations that can be efficiently computed by a variety of methods [58]. In Fig. 2 we have plotted $(\Delta\hat{L})^2_{2n}$ and $(\Delta\hat{E})^2_{2n}$ as functions of the Lagrange multiplier q.

D. Intelligent states: Asymptotic limits

To better understand Fig. 2 we first concentrate on the limit of small q [i.e., large $(\Delta\hat{E})^2_{2n}$]. We expand $\mathrm{ce}_{2n}(\eta,q)$ in powers of q and retain only linear terms [56]

$$\mathrm{ce}_0(\eta,q) = \frac{1}{\sqrt{2}}\left(1 - \frac{q}{2}\cos(2\eta)\right),$$

$$\mathrm{ce}_2(\eta,q) = \cos(2\eta) - q\left(\frac{\cos(4\eta)}{12} - \frac{1}{4}\right),$$

$$\mathrm{ce}_{2n}(\eta,q) = \cos(2\eta) - \frac{q}{4}\left(\frac{\cos[(2n+2)\eta]}{2n+1}\right.$$
$$\left. - \frac{\cos[(2n-2)\eta]}{2n-1}\right), \quad n \geq 2. \quad (2.43)$$

This leads to

$$(\Delta\hat{L})^2_2 = 1 - \frac{5q^2}{48} + O(q^4), \quad (\Delta\hat{E})^2_2 = 1 - \frac{25q^2}{144} + O(q^4),$$

$$(\Delta\hat{L})^2_{2n} = n^2 - \frac{q^2}{8(4n^2-1)} + O(q^4),$$

$$(\Delta\hat{E})^2_{2n} = 1 - \frac{q^2}{4(4n^2-1)^2} + O(q^4), \quad n \neq 1, \quad (2.44)$$

showing a quadratic behavior which can be appreciated in Fig. 2.

In the opposite limit of large q [small $(\Delta\hat{E})^2_{2n}$], we take the approximation in terms of Hermite polynomials [58]

$$\mathrm{ce}_{2n}(\eta,q) \propto e^{-u^2/4}H_{2n}\left(\frac{u}{\sqrt{2}}\right) + O(q^{-1/2}), \quad (2.45)$$

where $u=2q^{1/4}\cos\eta$. Apart from constant factors, the states (2.45) look like harmonic oscillator wave functions and we can use them to evaluate the variances analytically. The final expressions involve the modified Bessel functions $I_k(\sqrt{q})$, but the crucial fact is that the following simple asymptotic expressions hold:

$$(\Delta\hat{L})^2_{2n} = \frac{(4n+1)}{4}\sqrt{q} + O(q^0),$$

$$(\Delta\hat{E})^2_{2n} = \frac{4n+1}{\sqrt{q}} + O(q^{-1}), \quad (2.46)$$

showing a square-root behavior that is also apparent from Fig. 2. The range of moderate values of q, where the transition between the quadratic (small q) and the square-root (large q) regions happens, is magnified in the inset. According to Eq. (2.46), with increasing q the uncertainty product $(\Delta\hat{L})_{2n}(\Delta\hat{E})_{2n}$ approaches a constant value depending exclusively on the mode index n; $\lim_{q\to\infty}(\Delta\hat{L})_{2n}(\Delta\hat{E})_{2n}=(4n+1)/2$. These asymptotic limits, confirmed in Fig. 2, identify the fundamental mode $n=0$ as the minimum-uncertainty state for

all the values of the parameter q. Henceforth, we always refer to the fundamental Mathieu mode, unless the mode index is explicitly given.

Finally, let us note that, from Eq. (2.43), it follows immediately that when $q \to 0$ the probability distribution for this fundamental mode is $p(\phi) \propto [1 - q \cos(\phi)/2]^2 \simeq \exp(-q \cos \phi)$; while when $q \to \infty$, according to Eq. (2.45), we have $H_0(u/\sqrt{2}) = 1$ and $p(\phi) \propto \exp[-2\sqrt{q} \cos^2(\phi/2)] \propto \exp(-\sqrt{q} \cos \phi)$. We therefore get the interesting result that

$$p(\phi) \propto |ce_0(\eta, q)|^2 \simeq \begin{cases} e^{-q \cos \phi}, & q \to 0, \\ e^{-\sqrt{q} \cos \phi}, & q \to \infty, \end{cases} \quad (2.47)$$

and hence the optimal states with very sharp and nearly flat angular profiles attain the von Mises shape.

E. Suboptimal states

Up to now we have investigated extremal states that will be used in the experiments as an ultimate calibration to assess the performance of our setup. Here, we compare these extremal states with suboptimal ones. There are plenty of possible candidates for that; we will select a few examples that can be easily prepared and intuitively grasp various features of "a well-localized angle."

The wedge structure is our first representative. The aperture function possesses sharp edges and may be defined in the angle representation as

$$\Psi(\phi) = \begin{cases} 1/\sqrt{\alpha}, & |\phi| \leq \alpha/2, \\ 0, & |\phi| > \alpha/2, \end{cases} \quad (2.48)$$

α being the opening angle of the wedge. The probability distribution of angular momentum $p_m = |\Psi_m|^2$ can be calculated using Eq. (2.7), and one finds

$$(\Delta \hat{L})^2 \to \infty,$$

$$p_m = \frac{\alpha}{2\pi} \frac{\sin^2(m\alpha/2)}{(m\alpha/2)^2} \quad \text{(wedge)},$$

$$(\Delta \hat{E})^2 = 1 - \frac{4}{\alpha^2} \sin^2(\alpha/2). \quad (2.49)$$

Similarly to the Fraunhofer diffraction pattern observed behind a rectangular slit, the variance $(\Delta \hat{L})^2$ is infinite due to the heavy tails of the sinc distribution and thus the angle–angular-momentum uncertainty relation is trivially satisfied for (2.48). In spite of this divergence, the experimenter cannot establish this simple fact from a finite data set: in general, the sampled angular-momentum uncertainty will grow with the amount of data acquired. Most of the detected m fall within the central peak $|m| \leq 2\pi/\alpha$ of the distribution, which tends to regularize the unbounded uncertainty product.

As another candidate for a simple single-peaked angular distribution we choose the state

$$\Psi(\phi) = \begin{cases} \sqrt{\dfrac{2}{\pi\alpha}} \cos(\phi/\alpha), & |\phi| \leq \pi\alpha/2, \\ 0, & |\phi| > \pi\alpha/2, \end{cases} \quad (2.50)$$

that is, the positive cosine half wave stretched to the interval $-\pi\alpha/2 \leq \phi \leq \pi\alpha/2$, so that $\alpha \leq 2$. The following discussion is valid even for $\alpha > 2$ provided the cosine half wave, which now spans an interval of width larger than 2π, is wrapped onto the unit circle. Since the delimiting aperture has no sharp edges, one can expect more regular results. A straightforward calculation yields

$$(\Delta \hat{L})^2 = 1/\alpha^2,$$

$$p_m = \frac{4\alpha \cos^2(\pi m \alpha/2)}{\pi^2 (m^2 \alpha^2 - 1)^2} \quad \text{(cosine)},$$

$$(\Delta \hat{E})^2 = 1 - \frac{64 \sin^2(\pi\alpha/2)}{\pi^2 \alpha^2 (\alpha^2 - 4)^2}. \quad (2.51)$$

At first sight, the angular-momentum distribution in Eq. (2.51) has a sinclike shape with infinitely many side lobes, which strongly resembles the one in Eq. (2.49). However, here the higher-order contributions to the angular-momentum variance are negligible and both uncertainties appear to be finite. Notice that the parameter α has now a very simple physical meaning: it is inversely proportional to the angular-momentum uncertainty.

Next, we consider the von Mises wave function

$$\Psi(\phi) = \frac{1}{\sqrt{2\pi I_0(1/\alpha)}} e^{\cos \phi/(2\alpha)}, \quad (2.52)$$

α being a monotonic function of the angular width. According to Eq. (2.47), the relevant uncertainties,

$$(\Delta \hat{L})^2 = \frac{I_1(1/\alpha)}{4\alpha I_0(1/\alpha)},$$

$$p_m = \frac{I_m^2(1/2\alpha)}{I_0(1/\alpha)} \quad \text{(von Mises)},$$

$$(\Delta \hat{E})^2 = 1 - \frac{I_1^2(1/\alpha)}{I_0^2(1/\alpha)}, \quad (2.53)$$

can also be taken (with an appropriate fitting of the parameter α) as excellent approximations to the uncertainties of the optimal Mathieu states, especially in the regions of small and large variances.

Finally, we evaluate the uncertainties of the truncated Gaussian

$$\Psi(\phi) = [\pi \, \text{erf}^2(\pi\alpha)/\alpha^2]^{-1/4} e^{-\alpha^2 \phi^2/2}, \quad (2.54)$$

which minimizes the uncertainty product for angular momentum and angle, the latter in the sense of ordinary variance [26,27]. Such states become suboptimal when the variance is replaced by a periodic measure, such as the circular variance advocated in this paper:
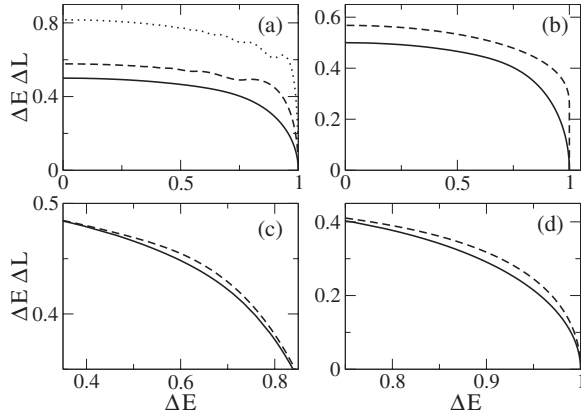
FIG. 3. Theoretical uncertainty products for angle and angular-momentum variables calculated for (a) wedge angle, (b) cosine, (c) von Mises, and (d) truncated normal distributions. In all panels the solid line denotes the optimal uncertainty product generated by the intelligent Mathieu wave function. In (a) the broken and dotted lines correspond to p_m truncated at the first and second minimum, respectively.

$$(\Delta\hat{L})^2 = \frac{\alpha^2}{2}\left[1 - \frac{2\sqrt{\pi}\alpha e^{-\pi^2\alpha^2}}{\mathrm{erf}(\pi\alpha)}\right],$$

$$p_m = \frac{e^{-m^2/\alpha^2}\left\{\mathrm{Re}\left[\mathrm{erf}\left(\frac{\pi\alpha^2 + im}{\sqrt{2}\alpha}\right)\right]\right\}^2}{\sqrt{\pi}\alpha\,\mathrm{erf}^2(\pi\alpha)} \quad \text{(truncated)},$$

$$(\Delta\hat{E})^2 = 1 - \frac{e^{-1/(2\alpha^2)}\left\{\mathrm{Re}\left[\mathrm{erf}\left(\frac{2\pi\alpha^2 + i}{2\alpha}\right)\right]\right\}^2}{\mathrm{erf}^2(\pi\alpha)}, \qquad (2.55)$$

where $\mathrm{erf}(z)$ is the error function.

Figure 3 shows the comparison of these four states with the optimal Mathieu one. As already mentioned, the measured uncertainty product for the wedge distribution grows with the amount of data acquired, since more and more side maxima are sampled [see Fig. 3(a)]. On the other hand, the uncertainty product of the cosine distribution in Fig. 3(b) is well defined and lies well above the quantum limit given by the Mathieu profile. In agreement with the asymptotic analysis of the previous section, the uncertainty product for the von Mises angular distribution falls very close to the optimal curve: only at intermediate angular spreads $\Delta\hat{E}$ do we see a significant deviation from the standard quantum limit, while for the truncated Gaussian states the deviation is larger and shifts toward higher values of $\Delta\hat{E}$. The point is whether the currently available measurements have sufficient resolution to discriminate between the optimal and suboptimal states mentioned above. This question is addressed in the next two sections.

III. MEASUREMENT OF THE ORBITAL ANGULAR MOMENTUM

A. Single vortex beam

The theory presented thus far can be applied to a variety of physical systems. Here, we consider a particularly appealing realization of a planar rotator in terms of optical beams.

Light beams can carry angular momentum, which comprises spin and orbital components that are associated with polarization and helical-phase fronts, respectively. In general, the spin and orbital contributions cannot be considered separately, but in the paraxial approximation both contributions can be measured and manipulated independently. We emphasize that this OAM is manifest at the macroscopic and single-photon levels and therefore paraxial quantum optics is the most convenient context in which to treat the OAM of light as a quantum resource.

In consequence, we can leave aside the spin part and consider the simplest scalar monochromatic beam carrying OAM: this is precisely a vortex beam; i.e., a beam whose phase varies in a corkscrewlike manner along the direction of propagation. The corresponding spatial amplitude can be written as

$$U(\mathbf{r}) = u(\mathbf{r})\exp(im\phi), \qquad (3.1)$$

where we have assumed that the beam propagates dominantly along the z axis, so we have cylindrical symmetry. According to the representation in Eq. (2.3), (3.1) is an eigenstate of $\hat{L}$ with eigenvalue m, which is also known as the topological charge (or helicity) of the vortex. To check this interpretation, note that the OAM density is also dominantly along the z axis and is given by $l = rS_\phi/c^2$, where S_ϕ is the azimuthal component of the Poynting vector. In a scalar theory, the time-averaged Poynting vector can be computed as $\mathbf{S} = is_0\omega(U^*\boldsymbol{\nabla} U - U\boldsymbol{\nabla} U^*)$, where s_0 is a constant (with units of m s). The density of the OAM of the vortex beam (3.1) then depends on its intensity $I = |U|^2$ and wave-front helicity and can be expressed in terms of its power P as

$$L = \frac{2\omega s_0 m P}{c^2}. \qquad (3.2)$$

If we divide now by the total energy density of the field we finally get that the OAM per photon can be interpreted precisely as the topological charge m. In this way, light beams prepared in OAM eigenstates can be used in quantum optics experiments in the same way as qudits.

B. Principle of the measuring method

A general scheme of our experimental method is sketched in Fig. 4. A collimated Gaussian beam with complex amplitude U_G illuminates an amplitude mask (with transmission coefficient t_A) performing an angular limitation of the beam. Immediately behind the mask, the beam transverse profile has a cake-slice shape given by $U_A = t_A U_G$. According to Eq. (2.7), the field azimuthal amplitude distribution results in a spread of the spectrum composed of vortex components with different topological charges and amplitudes. The beam propagates toward a spiral phase mask [with transmission
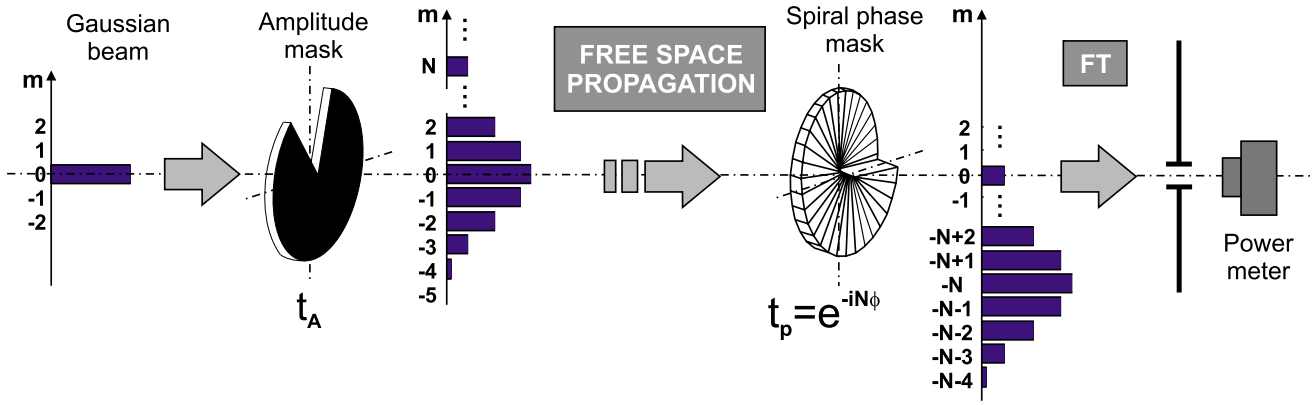
FIG. 4. (Color online) Principle of the measurement of the angular-momentum spectrum of the angular restricted field.

$t_P = \exp(-iN\phi)$] introducing a helicity $-N$. Behind the phase mask, the transmitted field is Fourier analyzed, so its spatial spectrum $\bar{U}_F$ can be obtained as

$$\bar{U}_F = \mathcal{F}[(t_A U_G * h)t_P], \tag{3.3}$$

where $\mathcal{F}$ denotes the Fourier transform, h is the impulse response function of free-space propagation between the amplitude and phase masks, and $*$ is the convolution product. The detected power can thus be interpreted as the spectral intensity collected at the power meter placed at the back focal plane of the lens used for the optical implementation of the Fourier transform.

As we show below, provided the aperture radius of the power meter is suitably chosen, the measured power can be used for estimating the OAM of the vortex mode with topological charge N in the field behind the amplitude mask. This procedure can be repeated with spiral phase masks of different topological charges, yielding the vortex distribution (i.e., angular-momentum spectrum) of the prepared angular-restricted beam. Several experimental realizations of this idea have been proposed and realized [28,29], differing in technical details and data analysis [59,60].

To put this in quantitative terms, let us first introduce a mode decomposition of the amplitude mask,

$$t_A = \sum_{m=-\infty}^{\infty} a_m \exp(im\phi), \tag{3.4}$$

where a_m are Fourier coefficients. We assume that the waist of the Gaussian beam (of width w_0) is placed exactly at the mask plane. The transmitted field propagates through free space, so the complex amplitude U_I of the field impinging on the spiral phase mask can be written in the form

$$U_I(\mathbf{r}) = \sum_{m=-\infty}^{\infty} a_m u_m(r,z)\exp(im\phi), \tag{3.5}$$

where we have used cylindrical coordinates (r,ϕ,z) and

$$u_m(r,z) = 2\pi u_0 i^m h_0 \exp\left(-\frac{ikr^2}{2z}\right)A_m(r,z),$$

$$A_m(r,z) = \int_0^\infty \exp(-\alpha r'^2)J_m(\beta rr')r'\,dr',$$

$$h_0 = \frac{i}{\lambda z}, \quad \alpha = \frac{1}{w_0^2} + \frac{ik}{2z}, \quad \beta = \frac{k}{z}. \tag{3.6}$$

Here J_m and u_0 denote the mth-order Bessel function of the first kind and a constant amplitude of the Gaussian beam, respectively, and z is the distance between amplitude and phase masks. The integration in (3.6) can be carried out and results in

$$A_m(r,z) = r\frac{Q}{\beta}\sqrt{\frac{\pi}{\alpha}}\exp(-Qr^2)[I_{1/2(m-1)}(Qr^2) - I_{1/2(m+1)}(Qr^2)], \tag{3.7}$$

where $Q = \beta^2/(8\alpha)$.

After transmission through the spiral phase mask, the Fourier transform of the field is performed optically and the spatial distribution at the back focal plane of the Fourier lens can be represented by the complex amplitude $\bar{U}_F$ given by

$$\bar{U}_F(\nu,\psi) = a_N[\bar{u}_N(\nu) - \bar{v}_N(\nu)] + \sum_{m=-\infty}^{\infty} a_m\bar{v}_m(\nu)\exp[i(m-N)\psi], \tag{3.8}$$

where

$$\bar{u}_m(\nu) = 2\pi\int_0^\infty u_m(r,z)J_0(2\pi\nu r)r\,dr,$$

$$\bar{v}_m(\nu) = 2\pi i^{(m-N)}\int_0^\infty u_m(r,z)J_{m-N}(2\pi\nu r)r\,dr. \tag{3.9}$$

Here (ν,ψ) are polar coordinates in the transverse Fourier plane (x_F,y_F), defined as $\nu = \sqrt{x_F^2+y_F^2}/(\lambda f')$ and $\psi = \arctan(y_F/x_F)$, f' being the lens focal length. The power captured by the circular aperture of the meter placed at the focal plane of the lens is given by
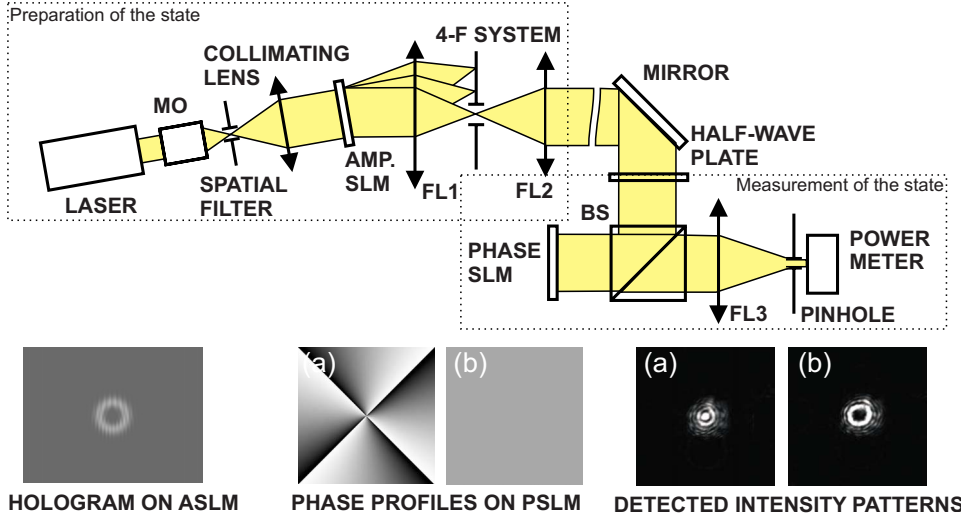
FIG. 5. (Color online) Experimental setup for the generation of beams with an arbitrary transverse profile and subsequent detection of their angular-momentum spectrum.

$$P = \int_0^{\nu_0} \int_0^{2\pi} |\bar{U}_F(\nu,\psi)|^2 \nu \, d\nu \, d\psi, \qquad (3.10)$$

where $\nu_0 = R/(\lambda f')$ and R denotes the aperture radius. By substituting (3.8) into (3.10), the detected power can be expressed as

$$P = P_N + P_C, \qquad (3.11)$$

where

$$P_N = 2\pi |a_N|^2 \int_0^{\nu_0} |\bar{u}_N|^2 \nu \, d\nu,$$

$$P_C = 2\pi \sum_{\substack{m=-\infty \\ m \neq N}}^{\infty} |a_m|^2 \int_0^{\nu_0} |\bar{v}_m|^2 \nu \, d\nu. \qquad (3.12)$$

This power appears to be composed of two terms. The first term P_N represents the power carried by the vortex mode of topological charge N. The second term P_C is a cross talk that represents disturbing contributions of the remaining vortex components and it can be reduced by a convenient choice of the aperture radius R of the power meter. This possibility follows directly from Eq. (3.8), since $|\bar{u}_N(0)|^2 \neq 0$ and has its maximum in the middle of the receiving aperture, while $|\bar{v}_m(0)|^2 = 0$ for $m \neq N$. The spectral intensity of the vortex whose power is measured creates a sharply peaked bright spot at the Fourier plane; meanwhile, the spectral intensities contributing to the cross-talk power have an annular form. These different spatial shapes enable an optimal choice of the radius of the receiving aperture. In this case, both the power lost of the measured vortex and the influence of the cross talk are minimized.

IV. EXPERIMENTAL RESULTS

To verify our theory, the angle–angular-momentum uncertainty products were experimentally measured on various light beams. Given the small difference between the optimal Mathieu beams and other suboptimal single-peaked angular

distributions, such a measurement is also an indicator of the resolution attainable with the present commercially available technology.

Figure 5 shows our setup. The beam generated by the laser (Verdi V2, 532 nm, 20 mW) is spatially filtered, expanded, and collimated by the lens and impinges on the hologram generated by the amplitude spatial light modulator (SLM) (CRL Opto, 1024×768 pixels). The bit map of the hologram is computed as an interference pattern of the tested state (with the desired angular amplitude distribution) and an inclined reference plane wave. After illuminating the hologram with the collimated beam, the Fourier spectrum of the transmitted beam is localized at the back focal plane of the first Fourier lens FL_1. It consists of three diffraction orders $(-1,0,+1)$. The undesired 0 and -1 orders are removed by a spatial filter. After inverse Fourier transformation, performed by the second Fourier lens FL_2, a collimated beam with the required complex amplitude profile $U_A = t_A U_G$ is obtained. This completes the state preparation.

The analysis begins by reflecting the prepared field U_A at a phase SLM (Boulder, 512×512 pixels), whose reflectivity is proportional to $t_P \propto e^{-iN\phi}$. As discussed in the previous section, after the Fourier transformation of the reflected field, the spectral component whose helicity was eliminated by the phase SLM gives rise to a bright spot [Fig. 5(a)], while the other components have an annular intensity distribution [Fig. 5(b)]. The vortex components of the spiral spectrum can be subsequently selected by the phase SLM and their OAM determined by a power measurement performed with an optimal aperture size of the power meter. To suppress cross talk, the calibrating response functions were acquired for each phase mask.

After the setup was carefully aligned using Laguerre-Gauss beams, transverse amplitude distributions of different shapes and angular variances were generated. Each beam was then scanned for values of helicities in the range of $m \in [-15, 15]$. A typical transverse intensity profile and the corresponding measured raw data are shown in Fig. 6.

In addition, the response functions were measured for pure vortex modes (see Fig. 7). For an ideal detection, the pure vortex mode with the topological charge N should have
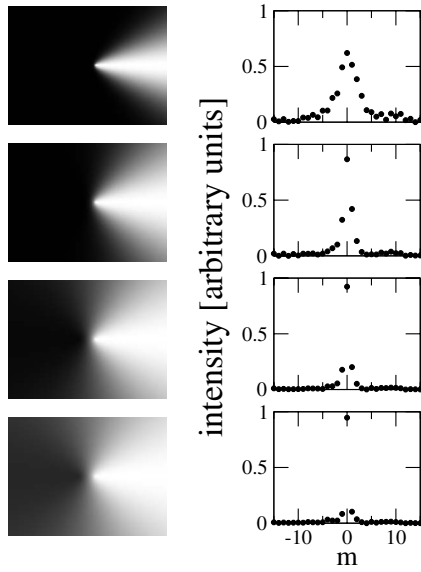
FIG. 6. Preparation and measurement of Mathieu states having circular variances (from top to bottom) $\Delta\hat{E}=0.31$, 0.54, 0.79, and 0.91. Left: computed intensity distribution; right: measured angular-momentum spectrum (in arbitrary units).

a δ-like angular momentum spectrum with a sharp peak at $m=N$. Any real detection scheme suffers from cross talk between modes, which tends to broaden the measured spectra in Fig. 6; this effect becomes more pronounced for larger helicities ($m>4$). It can be seen, from comparing Figs. 6 and 7, that the reliability of the measured spectrum decreases from the center ($m=0$) to the edges and that beams of smaller variances have broader angular spectra and vice versa. Hence the reliability of experimentally determined uncertainty products is expected to increase with variance.

In the next step, the acquired response functions were used to increase the resolution of our detection scheme. Since the measured spectra could be considered to be convolutions of true angular spectra and known response functions, we could apply an inverse transformation to minimize the effect of cross talk. Then, the angular-momentum variances were estimated by fitting the deconvoluted data to the theoretically calculated distributions. The family of distribu-
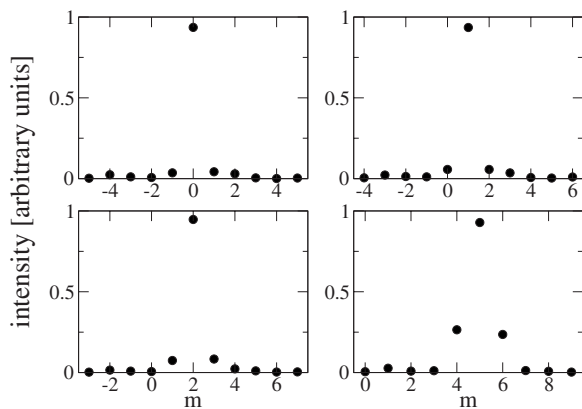

FIG. 7. Measured response functions of our detection scheme for pure vortex modes of helicities $m=0$, 1, 2, and 5.
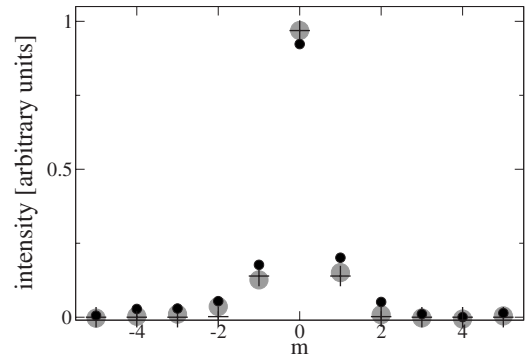

FIG. 8. Analysis of measured angular-momentum spectrum of a Mathieu beam of $\Delta\hat{E}=0.79$. Raw data (small black circles), deconvoluted data (large gray circles), and best fit with a theoretical distribution (+ symbols) are shown.

tions used for fitting experimental data was parametrized by an overall normalization factor and a parameter characterizing the angular width of the corresponding state. For example, the fitting procedure applied to data measured on a Mathieu beam yielded the value of parameter q, which was then used to determine the variance of angular momentum via Eq. (2.41). This stage of analysis is illustrated in Fig. 8. In addition to getting $(\Delta\hat{L}^2)$ the quality of the best fit was quantified, enabling error bars to be placed on the resulting uncertainty products.

Experimental results are summarized in Fig. 9. Given the resolution of the setup (indicated by error bars), the obtained uncertainty products fit the theoretical predictions quite well. As anticipated, the resolution is not uniform and gets better in the region of large variances.

Inspection of the upper panels of Fig. 9 shows that the measurements of the optimal Mathieu and von Mises beams
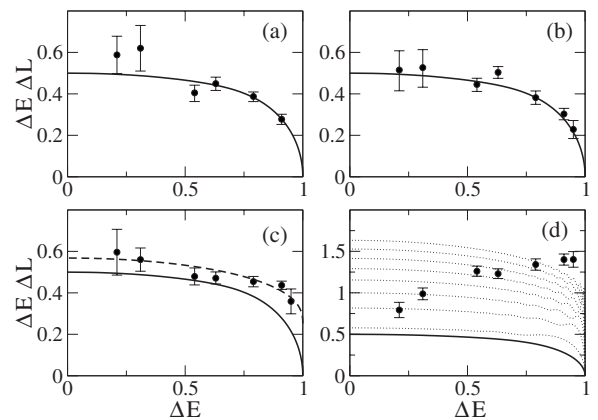

FIG. 9. Experimentally determined uncertainty products for angle and angular momentum. The following angular distributions of beam amplitude in the transverse plane were measured: (a) Mathieu distribution of Eq. (2.38), (b) von Mises distribution of Eq. (2.52), (c) cosine distribution of Eq. (2.50), and (d) wedge distribution of Eq. (2.48). Experimentally obtained uncertainty products are denoted by circles. For comparison, theoretical uncertainty products of the optimal Mathieu (solid line), cosine (broken line), and wedge angular distributions whose angular momentum spectra have been truncated at the first, second, etc. minimum (dotted lines) are also shown.

yield very similar results. This could be expected, since the difference between the uncertainty products of these two beams [see Fig. 3(c)] is below the resolution of the present setup. The cosine and wedge angle distributions in the bottom panels of Fig. 9 can be discriminated from the optimum more easily. While the suboptimality of the cosine distribution is confirmed only for moderate to large variances $\Delta \hat{E}$ > 0.75, the wedge angular shape shows entirely different behavior: the uncertainty product increases with the variance. This tendency of the wedge distribution can be readily explained: as the variance gets larger, more and more side maxima of the sinclike angular momentum spectrum fall into the detected window $m \in [-15, 15]$, yielding a corresponding growth of the uncertainty product.

V. CONCLUSIONS

In conclusion, we have formulated rigorous uncertainty relations for angle and angular momentum based on the circular variance as a proper statistical measure of angular error. Fundamental Mathieu states were identified as intelligent states under the constraint of given uncertainty either in angle or in angular momentum. In this sense, the Mathieu states provide the optimal distribution of information between the two observables, with possible applications in information processing. An optical test of the uncertainty relations was performed by using spatial light modulators for both the beam preparation and analysis.

Although the present experiment nicely confirmed our theory, the resolution of the present setup was not sufficient for observing finer details in the angular-momentum representation of light beams. Further improvements both in the detection scheme and in hardware are highly desirable. Our scheme is conceptually simple but suffers from cross talk and artifacts, especially at large helicities. Better detection schemes based on direct sensing of the beam wave front could perhaps solve this problem. Concerning beam manipulation, the spatial light modulators used in our experiment, though very flexible and easy-to-use devices, also have their drawbacks, namely, small light efficiencies and pixelated structures. A possible future upgrade of the experimental setup lies in employing an optically addressed SLM.

[1] V. Peřinova, A. Lukš, and J. Peřina, *Phase in Optics* (World Scientific, Singapore, 1998).

[2] A. Luis and L. L. Sánchez-Soto, Prog. Opt. **44**, 421 (2000).

[3] H. A. Kastrup, Phys. Rev. A **73**, 052104 (2006).

[4] L. Allen, S. M. Barnett, and M. J. Padgett, *Optical Angular Momentum* (Institute of Physics Publishing, Bristol, 2003).

[5] L. Allen, M. W. Beijersbergen, R. J. C. Spreeuw, and J. P. Woerdman, Phys. Rev. A **45**, 8185 (1992).

[6] Z. Bouchal and R. Čelechovský, New J. Phys. **6**, 131 (2004).

[7] G. Gibson, J. Courtial, M. J. Padgett, M. Vasnetsov, V. Pas'ko, S. M. Barnett, and S. Franke-Arnold, Opt. Express **12**, 5448 (2004).

[8] R. Čelechovský and Z. Bouchal, New J. Phys. **9**, 328 (2007).

[9] A. Mair, A. Vaziri, G. Weihs, and A. Zeilinger, Nature (London) **412**, 313 (2001).

[10] A. Vaziri, G. Weihs, and A. Zeilinger, J. Opt. B: Quantum Semiclass. Opt. **4**, S47 (2002).

[11] G. Molina-Terriza, A. Vaziri, J. Řeháček, Z. Hradil, and A. Zeilinger, Phys. Rev. Lett. **92**, 167903 (2004).

[12] N. K. Langford, R. B. Dalton, M. D. Harvey, J. L. O'Brien, G. J. Pryde, A. Gilchrist, S. D. Bartlett, and A. G. White, Phys. Rev. Lett. **93**, 053601 (2004).

[13] S. S. R. Oemrawsingh, X. Ma, D. Voigt, A. Aiello, E. R. Eliel, G. W. 't Hooft, and J. P. Woerdman, Phys. Rev. Lett. **95**, 240501 (2005).

[14] L. Marrucci, C. Manzo, and D. Paparo, Phys. Rev. Lett. **96**, 163905 (2006).

[15] G. Molina-Terriza, J. P. Torres, and L. Torner, Nat. Phys. **3**, 305 (2007).

[16] M. M. Nieto, Phys. Rev. Lett. **18**, 182 (1967).

[17] J. Zak, Phys. Rev. **187**, 1803 (1969).

[18] C. T. Whelan, J. Phys. A **13**, L181 (1980).

[19] D. Loss and K. Mullen, J. Phys. A **25**, L235 (1992).

[20] Y. Ohnuki and S. Kitakado, J. Math. Phys. **34**, 2827 (1993).

[21] S. Szabó, Z. Kis, P. Adam, and J. Janszky, Quantum Opt. **6**, 527 (1994).

[22] V. A. Kostelecký and B. Tudose, Phys. Rev. A **53**, 1978 (1996).

[23] K. Kowalski and J. Rembieliński, J. Phys. A **35**, 1405 (2002).

[24] J. Y. Bang and M. S. Berger, Phys. Rev. D **74**, 125012 (2006).

[25] R. Bluhm, V. A. Kostelecký, and B. Tudose, Phys. Rev. A **52**, 2234 (1995).

[26] S. Franke-Arnold, S. M. Barnett, E. Yao, J. Leach, J. Courtial, and M. Padgett, New J. Phys. **6**, 103 (2004).

[27] D. T. Pegg, S. M. Barnett, R. Zambrini, S. Franke-Arnold, and M. Padgett, New J. Phys. **7**, 62 (2005).

[28] J. Leach, M. J. Padgett, S. M. Ba, Urnett, S. Franke-Arnold, and J. Courtial, Phys. Rev. Lett. **88**, 257901 (2002).

[29] Z. Hradil, J. Rehacek, Z. Bouchal, R. Čelechovský, and L. L. Sánchez-Soto, Phys. Rev. Lett. **97**, 243601 (2006).

[30] J. C. Gutiérrez-Vega, M. D. Iturbe-Castillo, and S. Chávez-Cerda, Opt. Lett. **25**, 1493 (2000).

[31] J. C. Gutiérrez-Vega, R. M. Rodríguez-Dagnino, M. A. Meneses-Nava, and S. Chávez-Cerda, Am. J. Phys. **71**, 233 (2003).

[32] M. A. Bandrés, J. C. Gutiérrez-Vega, and S. Chávez-Cerda, Opt. Lett. **29**, 44 (2004).

[33] P. Carruthers and M. M. Nieto, Rev. Mod. Phys. **40**, 411

(1968).

[34] G. G. Emch, *Algebraic Methods in Statistical Mechanics and Quantum Field Theory* (Wiley, New York, 1972).

[35] J. M. Lévy-Leblond, Ann. Phys. (N.Y.) **101**, 319 (1976).

[36] D. Judge and J. Lewis, Phys. Lett. **5**, 190 (1963).

[37] W. H. Louisell, Phys. Lett. **7**, 60 (1963).

[38] G. W. Mackey, *Mathematical Foundations of Quantum Mechanics* (Benjamin, New York, 1963).

[39] C. Helstrom, *Quantum Detection and Estimation Theory* (Academic, New York, 1976).

[40] U. Leonhardt, J. A. Vaccaro, B. Böhmer, and H. Paul, Phys. Rev. A **51**, 84 (1995).

[41] A. Luis and L. L. Sánchez-Soto, Eur. Phys. J. D **3**, 195 (1998).

[42] D. Mumford, *Tata Lectures on Theta I* (Birkhauser, Boston, 1983).

[43] *Handbook of Mathematical Functions*, edited by M. Abramowitz and I. A. Stegun (Dover, New York, 1984).

[44] K. V. Mardia and P. E. Jupp, *Directional Statistics* (Wiley, Chichester, UK, 2000).

[45] R. Barakat, J. Opt. Soc. Am. A **4**, 1213 (1987).

[46] A. Klimov and S. Chumakov, Phys. Lett. A **235**, 7 (1997).

[47] A. Perelomov, *Generalized Coherent States and Their Applications* (Springer, Berlin, 1986).

[48] J. A. González and M. A. del Olmo, J. Phys. A **31**, 8841 (1998).

[49] B. C. Hall and J. J. Mitchell, J. Math. Phys. **43**, 1211 (2002).

[50] K. Kowalski, J. Rembieliński, and L. C. Papaloucas, J. Phys. A **29**, 4149 (1996).

[51] C. R. Rao, *Linear Statistical Inference and its Applications* (Wiley, New York, 1965).

[52] E. Breitenberger, Found. Phys. **15**, 353 (1985).

[53] J. B. M. Uffink, Ph.D. thesis, University of Utrecht, 1990.

[54] I. Bialynicki-Birula, M. Freyberger, and W. Schleich, Phys. Scr., T **48**, 113 (1993).

[55] G. W. Forbes and M. A. Alonso, Am. J. Phys. **69**, 340 (2001).

[56] N. W. McLachlan, *Theory and Application of Mathieu Functions* (Oxford University Press, New York, 1947).

[57] T. Opatrný, J. Phys. A **28**, 6961 (1995).

[58] D. Frenkel and R. Portugal, J. Phys. A **34**, 3541 (2001).

[59] M. V. Vasnetsov, J. P. Torres, D. V. Petrov, and L. Torner, Opt. Lett. **28**, 2285 (2003).

[60] G. Molina-Terriza, L. Rebane, J. P. Torres, L. Torner, and S. Carrasco, J. Eur. Opt. Soc. Rapid Publ. **2**, 07014 (2007).